Marine Geology
June 2009, Volume 261, Issues 1-4, Pages 92-104
http://dx.doi.org/10.1016/j.margeo.2008.10.008

Multi-disciplinary investigation of fluid seepage on an unstable margin: The case of the Central Nile deep sea fan

G. Bayon[a, *], L. Loncke[b], S. Dupré[a, c], J.-C. Caprais[d], E. Ducassou[e], S. Duperron[f], J. Etoubleau[a], J.-P. Foucher[a], Y. Fouquet[a], S. Gontharet[g], G.M. Henderson[h], C. Huguen[i], I. Klaucke[j], J. Mascle[k], S. Migeon[k], K. Olu-Le Roy[d], H. Ondréas[a], C. Pierre[g], M. Sibuet[d], A. Stadnitskaia[l] and J. Woodside[c]

[a] Département Géosciences Marines, IFREMER, Brest, France
[b] UMR 8110, Université de Picardie Jules Verne, Amiens, France
[c] Sedimentology and Marine Geology Department, Vrije Universiteit, Amsterdam, The Netherlands
[d] Département Etude des Ecosystèmes Profonds, IFREMER, Brest, France
[e] UMR 5805 EPOC, Université de Bordeaux 1, France
[f] UMR 7138, Université Pierre et Marie Curie, Paris, France
[g] LOCEAN, Université Pierre et Marie Curie, Paris, France
[h] Department of Earth Sciences, University of Oxford, UK
[i] LEGEM, Université de Perpignan, Perpignan, France
[j] IFM-GEOMAR, Kiel, Germany
[k] Géosciences Azur UMR 6526, Villefranche-sur-mer, France
[l] Royal Netherlands Institute for Sea Research, Texel, The Netherlands

*: Corresponding author : G. Bayon, Tel.: +33 2 98 22 46 30; fax: +33 2 98 22 45 70, email address : Germain.Bayon@ifremer.fr

Abstract:

We report on a multidisciplinary study of cold seeps explored in the Central Nile deep-sea fan of the Egyptian margin. Our approach combines *in situ* seafloor observation, geophysics, sedimentological data, measurement of bottom-water methane anomalies, pore-water and sediment geochemistry, and ^{230}Th/U dating of authigenic carbonates. Two areas were investigated, which correspond to different sedimentary provinces. The lower slope, at ~ 2100 m water depth, indicates deformation of sediments by gravitational processes, exhibiting slope-parallel elongated ridges and seafloor depressions. In contrast, the middle slope, at not, vert, ~ 1650 m water depth, exhibits a series of debris-flow deposits not remobilized by post-depositional gravity processes.

Significant differences exist between fluid-escape structures from the two studied areas. At the lower slope, methane anomalies were detected in bottom-waters above the depressions, whereas the adjacent ridges show a frequent coverage of fractured carbonate pavements associated with chemosynthetic vent communities. Carbonate U/Th age dates (~ 8 kyr BP), pore-water sulphate and solid phase sediment data suggest that seepage activity at those carbonate ridges has decreased over the recent past. In contrast, large (~ 1 km2) carbonate-paved areas were discovered in the middle slope, with U/Th isotope evidence for ongoing carbonate precipitation during the Late Holocene (since ~ 5 kyr BP at least).

Our results suggest that fluid venting is closely related to sediment deformation in the Central Nile margin. It is proposed that slope instability leads to focused fluid flow in the lower slope and exposure of 'fossil' carbonate ridges, whereas pervasive diffuse flow prevails at the unfailed middle slope.

Keywords: Nile; continental margin; cold seep; U-Th; authigenic carbonate

1 – Introduction

Submarine pockmarks are widespread features on continental margins, which are often related to seepage of gas-rich fluids at the seafloor and/or to the presence of gas hydrates in marine sediments (e.g. Hovland and Judd, 1988; Judd and Hovland, 2007). Over recent years, there has been much interest in the study of seafloor pockmarks because they represent potential pathways for important quantities of gas from sediments to the ocean and, perhaps, to the atmosphere (e.g. Vogt et al., 1999; Paull et al., 2002; Ussler et al., 2003; Dimitrov and Woodside, 2003; Hovland et al., 2002, 2005; Gay et al., 2006). In active seepage sites, expulsion of gas-rich fluids commonly supports the development of chemosynthetic communities and the formation of authigenic carbonates, both of which are of interest for the understanding of biogeochemical and microbiological processes related to fluid seeping.

Increasing evidence of vast submarine pockmark fields in areas of destabilised seafloor sediments has questioned the relationship between slope instability and fluid circulation on continental margins (e.g. Hovland et al., 2002; Gay et al., 2004; Lastras et al., 2004; Loncke et al., 2004; Trincardi et al., 2004). Are sediment slides responsible for fluid release on the seafloor or, instead, does fluid circulation within margin sediments favour mass movements? A recent compilation of published dates for major submarine failures occurring in the North Atlantic area has shown that most sediment failures took place during two distinct periods over the last 45,000 years: the Bølling-Ållerød (15 – 13 ka) and the Preboreal (11 – 8 ka), which correlate with peaks of enhanced atmospheric methane concentrations recorded in ice cores (Maslin et al., 2004). It has been speculated that dissociation of gas hydrates in marine sediments, in response to environmental changes, has been instrumental in triggering such sediment failures, possibly releasing significant quantities of methane into the atmosphere (e.g. Paull et al., 2000; Nisbet, 2002; Kennett et al., 2002; Mienert et al., 2005). Isotopic records of atmospheric CH_4 in ice cores suggest, however, that marine gas hydrate reservoirs have remained stable during the Late Quaternary (Sowers, 2006). In-depth investigations of selected key regions are now needed, however, to bring further insights on the mechanisms linking slope instabilities, fluid circulation and methane emission on continental margins (e.g. Mienert, 2004).

Here, we report on a multidisciplinary study of cold seeps and mass movements explored off Egypt (Eastern Mediterranean basin), which brings interesting information on the relationship between fluid seepage and slope instabilities on continental margins. Fluid-related structures are particularly abundant in the central province of the Nile deep-sea fan, between 1500 and 2500 m water depth - an area where sediments are completely destabilised by gravitational processes (Loncke et al., 2002; Loncke et al., 2004). Selected targets of the Nile deep-sea fan were explored during two expeditions (Nautinil 2003 - R/V Atalante; Mimes 2004 - R/V Pelagia), funded through the MEDIFLUX project (ESF Euromargins Programme). This work represents a synthesis of *in situ* seafloor observation with the *Nautile* submersible, geophysical (3.5 kHz profiles, deep-tow sidescan sonar seafloor imagery), sedimentological and geochemical data (dissolved sulphate, elemental analyses, ^{230}Th/U carbonate ages), some of which include preliminary results.

2 – Geological setting

The Nile deep sea fan is a large sedimentary wedge, which has developed mainly since the Late Miocene in the eastern Mediterranean Sea (e.g. Salem, 1976). The morphology of the Nile deep sea fan results from the complex interplay between pre-Messinian inherited topography, salt-related deformation, and sediment gravity processes. Salt tectonism (e.g. diapirism, gravity spreading and gliding) on the Nile margin is related to the presence of a ductile Messinian salt layer within the sedimentary edifice (Mascle et al., 2000; Gaullier et al., 2000; Loncke et al., 2006). Sediment mass-wasting (e.g. slumping, debris flows) has occurred on the entire Nile fan, in response to various processes, such as salt-tectonism, sediment overloading and fluid circulation. In particular, the Central Nile Province is characterized by a highly destabilised seafloor surface, which shows repeated sediment failures and debris flows (Loncke et al., 2002; Loncke et al., 2004). Loncke et al. (2004) suggested that sediment instability in the Central Nile Province may be related to circulation of gas-rich fluids within sub-surface sediments.

A large number of seafloor structures related to fluid venting were recognised on the Nile margin during recent geophysical surveys (Fig. 1; Bellaiche et al., 2001; Loncke et al., 2002; Loncke et al., 2004). Numerous gas chimneys and associated mud volcanoes and cones were identified in Eastern (e.g. Isis, Amon, Osiris; see Fig. 1) and Western provinces. Many of these structures have been emplaced in areas where Messinian salt layers are absent in the sedimentary cover or have thinned down significantly, thereby allowing deep pre-Messinian fluids to migrate upward along major faults. Other smaller seafloor structures related to fluid venting were identified on the Nile margin from ship-borne multibeam acoustic images. They correspond to numerous highly-reflective patches, attributed to small pockmarks and/or mounds (Fig. 1; Loncke et al., 2004). Those patches are clustered in two areas (Fig. 1): in the Eastern province, in close proximity to gas chimneys; and in the Central Nile Province, associated with destabilized sediments. In the Central Province, those highly reflective acoustic patches occur mainly at water depths ranging from ~ 500 m down to 2500 m. One important objective of the MEDIFLUX project was to characterise those acoustic patches identified on ship-borne multibeam seafloor maps and to establish their relationship with fluid seepage and slope instability.

3 – Materials and Methods

3.1. Geophysics

An extensive set of geophysical data (3.5 kHz profiles, Simrad EM12-Dual and EM300-Dual multibeam echosounder and seismic data) was acquired during the Nautinil 2003 expedition, as well as during previous Géosciences-Azur cruises (PrismedII 1998, Fanil 2000 and Vanil 2004), which provided bathymetric and acoustic maps for the entire Nile deep sea fan (Loncke et al., 2004). Multibeam EM12- and EM-300 data were combined and processed at a grid size of 50m/pixel, using the Caraïbes software. High-resolution EdgeTech DTS-1 side-scan sonar data were acquired during the Mimes 2004 expedition. The deep tow side scan sonar was deployed and towed at around 100 m above the seafloor and operated at a 75-kHz frequency, with a 1500m wide swath of the seafloor.

3.2. *Nautile* dives

Nautile dives took place in two different areas on the Central Nile Province: 1) the lower slope, at ~ 2100 m water depth (dives NL6 and NL14; Fig. 1), and 2) the middle slope, at ~ 1650 m water depth (dive NL7; Fig. 2B,C). Microbathymetric profiles along each dive transect were acquired using *Nautile* sensors (pressure sensor and sounder). A methane sensor (Capsum METS) was installed on the Nautile frame to detect methane in bottom-waters. Note that concentrations measured with the methane sensor are qualitative only.

3.3. Sediment cores

A set of push-cores and blade-cores (i.e. a submersible-mounted corer equipped with a guillotine-like cutter, which allows efficient sampling of unconsolidated sediments) was collected in the Central Nile province during the *Nautile* dives. One piston core (NLK11) was also collected from the lower slope during the Nautinil cruise. The position of all sediment cores used for this study is given in Table 1 and shown in Figs. 1, 3B,C and 4. Push-cores NL14-PC1 and NL14-PC3 were retrieved in carbonate ridge areas (see description of fluid-venting structures in section 4.2). Push-core NL6-PC1 was collected from a small pockmark on the lower slope. The blade core NL7-BC1 is a reference core recovered in the middle slope, away from fluid venting structures. The lithological description for those cores is presented in Fig. 5. Hemipelagic sediments in the Nile deep sea fan correspond typically to reddish-brown foraminiferal and pteropod oozes (core NL7-BC1; uppermost part of cores NL14-PC1/3). In contrast, dark-grey sediments are encountered frequently at cold seep sites (core NL6-PC1; lower part of cores NL14-PC

1/3), which may contain small (mm- to cm- size) concretions of authigenic carbonates (Fig. 5).

3.4. Sediment geochemistry and pore water analyses

The inorganic geochemical composition of authigenic carbonates and sediments was determined by wavelength dispersive X-ray fluorescence (WD-XRF) analysis of fusion beads or compressed powder pellets for major and trace elements, respectively. Both total and oxidised (SO_4) sulphur contents of sediment samples were measured by XRF, allowing the determination of reduced sulphur concentrations (e.g. pyrite) by subtraction. Pore waters were extracted from core NL14-PC1 sediments by centrifuge. Dissolved sulphate concentrations were measured in 1:10 diluted solutions by ion chromatography with an accuracy better than 4%.

3.5. U/Th dating of authigenic carbonates

Bayon et al. (2007) reported ^{230}Th/U ages for a set of samples drilled across a carbonate crust recovered from the middle slope (NL7-CC2 crust; see location in Fig. 4), which provided evidence for continuous carbonate precipitation at that studied location over the last ~ 5000 years at least. In this study, we performed additional U-Th isotope measurements for two other carbonate crusts (NL6-CC1 and NL14-CC5; see location in Figs. 3B,C), collected from carbonate ridges in the lower slope. NL6-CC1 and NL14-CC5 crusts correspond to carbonate pavements characterized by a homogeneous matrix of terrigenous sediment (silt, clay), foraminifers and nannofossils, cemented by fine-grained aragonite (Gontharet et al., 2007).

Details on chemical and analytical procedures are presented elsewhere (Bayon et al., 2007), and a brief description is given here. Selected areas of carbonate crusts were hand-drilled carefully to obtain ~100 mg of carbonate powder. Carbonate samples were spiked with a mixed $^{236}U/^{229}Th$ spike prior to sample digestion. U and Th were then separated chemically using conventional anion exchange techniques. U and Th concentrations and isotope ratios were measured by multiple collector inductively coupled plasma mass spectrometry (MC-ICPMS) at the University of Oxford. Detrital contamination was typically too high for allowing calculation of ages using the conventional ^{230}Th age equation and required instead the use of isochron methods (e.g. Bourdon et al., 2003). For this approach, a sediment end-member was defined as the average of two sediments from the studied area (Bayon et al., 2007), assumed to be representative of the sediment fraction incorporated within the carbonate crusts.

4 – Results

4.1. Morphology of the Central Nile Province

New geophysical data acquired during the Nautinil cruise and other recent Geosciences-Azur expeditions allow to distinguish three distinct areas in the Central Nile Province, which are described briefly below (Fig. 1; Fig. 2):

a) The upper slope (between ~ 500 and 700 m water depth), characterised by the presence of a few large gas chimneys (up to 4 km in diameter) corresponding to the leakage of gas-rich fluids from poorly sealed hydrocarbon reservoirs (e.g. North Alex; Fig. 1). Numerous slides observed in deeper parts of the Central Nile Province initiate at the location of the gas chimneys (Loncke et al., 2004). Note that one *Nautile* dive took place in this area (i.e. North Alex chimney) during the Nautinil cruise, but those results are discussed elsewhere (Dupré et al., 2007).

b) The middle slope (between ~ 700 and 1650 m water depth), characterised by a series of transparent acoustic bodies (debris-flow deposits) overlapping surface sediments in the lower slope (Fig. 2A). The most recent debris-flow deposits in this area are overlain by a thin hemipelagic cover (~ 0.5 m), which suggests recent deposition. Ship-borne multibeam backscatter imagery reveals the presence of a few highly reflective patches in this area (Loncke et al., 2004).

c) The lower slope (between ~ 1650 and 2200 m water depth), characterised by rough and chaotic seafloor morphology. The sedimentary cover is deformed by repeated undulations (i.e. a succession of elongated ridges and troughs), between 300 to 1500 m wide, sub-parallel to the slope (Figs. 1, 2A,C). Loncke et al. (2002) interpreted those undulations as a result of creep and gliding processes, rather than sediment waves created by bottom currents. Examination of 3.5 kHz profiles (Fig. 2A; Loncke et al., 2002) also suggests that some ridges observed in this area correspond to small rotated blocks. This deformed sedimentary cover is about 10 to 50 m thick and is underlain by debris-flow deposits (Fig. 2A). In core NLK11 (see location in Fig. 1), debris-flow deposits occur at sediment depths below 12 m (Fig. 5). A large number of highly reflective patches were identified in this area (Loncke et al., 2004), some of which were investigated during the Nautinil cruise (Figs. 1 and 2).

4.2. Fluid venting structures

Microbathymetric profiles and maps for sediment facies and carbonate crust occurrences along each *Nautile* dive transect are shown in Figures 3 and 4, together with EM-300 Multibeam acoustic map (Fig. 3A) and side-scan sonar seafloor imagery (Fig. 4). Note that only the dive NL7 area (middle slope area) was surveyed by the EdgeTech deep tow sonar during the Mimes expedition. Combining geophysical data, *in situ* observation and microbathymetric profiles, four types of fluid venting structures can be identified in the lower slope and middle slope parts of the Central Nile province, which are described below.

4.2.1. Carbonate ridges (lower slope)

Three carbonate-paved areas were discovered on the lower slope during the *Nautile* dives, which correspond clearly to highly reflective patches (dark spots) on EM-300 multibeam mosaic (Fig. 3A). Microbathymetric profiles generated from the submersible sensors reveal that they correspond to aligned carbonate mounds, up to ~ 500 m long and 5 m high (Fig. 3B,C). Clearly, these carbonate-paved areas occur on top of the elongated ridges related to downslope mass movements (Fig. 2). Carbonate pavements were mainly covered by hemipelagic sediments (Fig. 6A). Fractured carbonate pavements were observed typically in topographically steep areas (Fig. 3B; Fig. 6B,C), often associated to faults with orientations ~ N70 and N160.

4.2.2. Elongated sediment depressions or troughs (lower slope)

In situ observations show the occurrence of large elongated depressions (~100 m long; 3 m deep) with signs of intense bioactivity, which occur in the immediate vicinity of carbonate ridges. The bioactivity is documented by the presence of light grey shell-rich sediments associated with numerous bioturbation mounds (Fig. 6G). Those depressions correspond to those slope-parallel troughs associated with undulations (Fig. 2), identified previously on multibeam bathymetric maps (Loncke et al., 2004). During the *Nautile* dives, many faults were observed in sediments (Fig. 3; Fig. 6H), with directions parallel (~N70) or perpendicular (~N160) to the slope (Fig. 3).

4.2.3. Other carbonate-paved areas (middle slope)

Two large (~ 1 km^2) carbonate-paved areas with irregular shapes and partly covered by sediments were identified from the side-scan sonar data in the middle slope (i.e. the large high backscatter areas shown as white patches in Fig. 4). The southernmost edge of one of these structures was visited during *Nautile* dive NL7 (Fig. 4), which corresponds to unfractured massive carbonate pavements. Bathymetric data acquired during the *Nautile* dive did not provide any evidence of topographic irregularities associated with carbonate pavements at that location.

4.2.4. Pockmarks

Numerous pockmarks were observed during the *Nautile* dives, both in the lower and middle slope areas. Pockmarks correspond to sub-circular depressions on the seafloor of variable size (typically 3-20 m across and up to 3 m deep), which can be isolated or occur as clusters (Figs. 4 and 6E). In the lower slope, pockmarks were observed in close vicinity to troughs (Fig. 3). Authigenic carbonate crusts occur typically in the central part of pockmarks, forming in some cases chimney-like build-ups (Fig. 6F). Shell debris, authigenic carbonate crusts and infilled burrows often accumulate within the depressions (Fig. 6F). In contrast to the reddish-brown foraminiferal and pteropod oozes characterising hemipelagic sediments on the Nile deep-sea fan (see reference core; Fig. 5), dark grey sediments were observed frequently in pockmarks (pushcore NL6-PC1; Fig. 5).

4.3. Biological observations

Several animal communities were observed during the *Nautile* dives in the two studied areas. Vestimentiferan tubeworms (Polychaeta: Siboglinidae) were often present in close association with carbonate crusts (Fig. 7), both in pockmarks and carbonate-paved areas. Two morphotypes of siboglinids were distinguished after examination of photographs and videos collected during the dives, but only one of them (assigned to the genus *Lamellibrachia*; Webb, 1969) was sampled successfully (Fig. 7A).

Numerous small mussels (length < ~1 cm) were found on carbonate crusts and associated sediments, occurring frequently inside small cavities within carbonate deposits. Those mussels have been shown recently to harbour 6 distinct types of bacterial symbionts, including sulphur- and methane-oxidizing bacteria, a diversity larger than reported from any other bivalve to date (Duperron et al, 2008). They display morphological similarities to *Idas modiolaeformis* (Sturany, 1896), a species reported at other eastern Mediterranean cold seep sites (Olu-Le Roy et al., 2004). Additional fauna associated with crusts includes anemones, serpulid polychetes and small galatheid crabs.

Empty bivalve shells were observed in carbonate-paved areas and pockmarks, but also in those large depressions close to carbonate ridges (P. Briand & K. Olu-Le Roy, pers. com.). These shells are similar to shells of *Isorropodon perplexum* (Vesycomyidae) and *Thyasira striata* (Thyasiridae), reported previously in the Nile deep-sea fan (Sturany, 1896) and on Anaximander mud volcanoes (Olu-Le Roy et al. 2004). A few living specimens of lucinids were sampled, which exhibit close morphological similarities to *Lucinoma kazani* (Anaximander mud volcanoes; Salas and Woodside 2002) and *Myrtea amorpha* (Mediterranean Ridge cold seeps; Olu-Le Roy et al. 2004). The former were shown recently to harbour sulphur-oxidizing bacteria (Duperron et al, 2007).

4.4. Detection of gas seeps

Methane profiles acquired in the lower slope with the Capsum METS sensor along selected dive transects are shown in Figs. 3B and C. Significant methane anomalies were measured in bottom waters above the large depressions associated with bioturbation mounds. Clearly, this shows that those troughs correspond to active sites of methane seepage. In contrast, no (dives NL6) or weak (dive NL14) methane anomalies were detected above carbonate-paved areas (Figs. 3B and C). In the middle slope, the Capsum sensor did not detect any methane anomaly (not shown here), but evidence for active fluid seepage is suggested by acoustic anomalies of side-scan sonar records of the water column attributed to gas bubbles (S. Dupré, personal communication; not shown here). One such acoustic gas anomaly was identified in close proximity to those large carbonate structures with irregular shapes.

At pockmarks, seepage of methane-rich fluids was inferred frequently by the presence of dark grey sediments (e.g. indicating the presence of an abundant organic fraction not decomposed). Evidence for on-going anaerobic oxidation of methane and bacterial sulphate reduction in one of those pockmarks was also given by a strong H_2S smell upon opening of core NL6-PC1 (Fig. 5).

4.5. Pore water and sediment geochemistry

Down-core high resolution profiles of CaO (wt. %), reduced and oxidized sulfur (wt. %) and barium (ppm) contents in sediment from push-cores NL14-PC1 and NL14-PC3 are presented in Fig. 8. Dissolved sulphate concentrations in pore waters (for core NL14-PC1 only) are also reported in Fig. 8. Pore water SO_4^{2-} concentrations are quasi-constant down to ~17 cm depth, with values (~ 30 mM) close to seawater concentrations.

In contrast to dissolved SO_4^{2-} concentrations, S concentrations in solid sediment phases increase from just a few centimeters (~ 7 cm) below the sediment/water interface (Fig. 8). In core NL14-PC1, enrichments of Ba and reduced S are related to the presence of barite (barium sulphate) and pyrite (iron sulfide), respectively. Mineralogical analyses and microscope observations reveal that authigenic gypsum (calcium sulphate) is also present within sediments.

4.6. Carbonate ^{230}Th/U ages

U-Th data for the two carbonate crusts analysed are listed in Table 2. Only one meaningful age was obtained for those lithified carbonate samples collected on the carbonate ridges (Table 2). This is due to an important ^{230}Th detrital contamination in those clay-rich samples. The calculated age for sample NL14-CC5 is ~ 7.9 ± 1.4 ka (Table 2).

5 – Discussion

5.1. Deformation style in the Central Nile margin

Significant differences were observed between the lower slope and the middle slope, which are summarised in Table 3. In the lower slope, downslope mass movements lead to formation of elongated ridges and troughs parallel to the slope (Loncke et al., 2002). Observation of numerous fractures in sediments during the *Nautile* dives provides direct evidence that active mass gravity processes occur in the lower slope. The presence of similar ridges and troughs at the base of continental margins has been extensively described in the literature (e.g. Mulder and Cochonat, 1996; van Weering et al., 1998; Lee and Chough, 2001; Gay et al., 2004). In the case of creep and downslope gliding, gravitational processes create typically two distinct structural domains: an extensional domain in the upper slope and a compressive domain located downslope (e.g. Allen, 1985; Pickering et al., 1989; Stow, 1994). In most cases, ridges and troughs form in the distal compressive parts of creeping or gliding sediment masses. By analogy, the lower slope on the Central Nile deep-sea fan could also correspond to a regional compressive domain. However, the occurrence of small rotated blocks in the lower slope indicates that extensional deformation takes place instead in this area, leading to faulting and associated rotated blocks. Most probably, it is likely that creeping of surface sediments in this lower slope domain also induces local compression, which could contribute, at least to some extent, to the formation of ridges and troughs.

In contrast to the lower slope, there is no direct evidence for active deformation processes taking place in the middle slope area. Most probably, the evidence that debris-flow deposits accumulated in the middle slope overlap surface sediments in the lower slope indicates that those two domains are decoupled.

5.2. Temporal evolution of fluid circulation

In cold seep environments, reduction of sulphate in pore waters is closely related to methane oxidation (Niewöhner et al., 1998; Borowski et al., 1999). The depth at which sulphate reduction occurs in sediments is controlled primarily by the upward flux of methane, being closer to the seafloor for high methane fluxes (Niewöhner et al., 1998; Borowski et al., 1999). Information on the temporal evolution of fluid venting at any site can be obtained by comparing pore water data (which give information on present-day fluid circulation) and solid sediment geochemical data (which may provide an integrated record of fluid seepage over the last few thousand years). In core NL14-PC1, the constant dissolved sulphate profile indicates that sulphate reduction does not proceed in the top sediment layer (~ 0-20 cm) at present. This suggests that methane-rich fluids probably do not circulate in sub-surface sediments at this location.

In contrast, the presence of authigenic sulphate (oxidized S) and sulfide (reduced S) minerals within sediment cores collected at carbonate ridges implies that reduction of pore-water sulphate was active at these sediment depths in the recent past. The dark grey sulfur- and barium-rich sediment layer in cores NL14-PC1/3 probably does not correspond to the Holocene Sapropel layer S1 (e.g., Olausson, 1961), which is buried at deeper sediment depths in the studied area (> 15 cm in our reference push-core NL7-

BC1; Fig. 5). The occurrence of S-rich minerals in NL14-PC1/3 sediments is probably related to oxidation of methane-rich fluids at that location in the recent past. At present, cold seep settings where sulphate reduction proceeds at only a few centimeters below the seafloor correspond to sites characterized by active fluid advection (e.g. see Haese et al., 2003 and references therein).

Absolute dating of authigenic carbonates with U-series also provides a means for reconstructing the evolution of cold seeps and associated fluid circulation through time (Teichert et al., 2003; Bayon et al., 2007). Certainly, additional U-Th isotope measurements would be needed to better constrain any spatial and temporal variations of fluid circulation activity in the lower slope. However, the U-Th age (~ 8 kyr BP) calculated for crust NL14-CC5 suggests that carbonate precipitation and hence fluid seepage was active at the studied carbonate ridge in the early Holocene. Taken together, our U-Th data and sediment geochemical profiles suggest therefore that the activity of fluid venting at carbonate ridge locations may have decreased over a recent period.

5.3. The origin of fluids

Fluids expelled at cold seeps on the Nile deep-sea fan may derive from shallow and/or deep sediment sources. Potential deep fluid sources include messinian and pre-messinian thermogenic hydrocarbon reservoirs (Abdel Aal et al., 2000; Samuel et al., 2003; Loncke et al., 2004). During the Nautinil expedition, the discovery of brine lakes on the seafloor (Menes Caldera, Western Nile province; Huguen et al., in revision) has provided clear evidence that fluids passing through or originating from deep evaporite deposits could be emitted on the seafloor in the Nile Delta area. Shallow fluid sources at cold seeps are most often related to formation of biogenic methane in superficial sediment layers; a consequence of the microbial degradation of organic matter during early diagenetic processes. Several organic-rich sediment layers (sapropels) have accumulated in Eastern Mediterranean basins during the Late Quaternary period (e.g., Olausson, 1961; De Lange and Ten Haven, 1983; Rossignol-Strick et al., 1982), which represent potential sources of methane-rich fluids to cold seeps in the Nile deep sea fan area. Fine-grained turbidites deposited on the deep-sea fan during the Late Quaternary may represent an additional source of biogenic methane. None of the data presented in this study can be used to discriminate the origin of fluids in the Central Nile area. However, stable isotope measurements ($\delta^{13}C$ and $\delta^{18}O$) on authigenic crusts collected during the Nautinil expedition (Gontharet et al., 2007) suggest that the fossil carbon source involved in carbonate precipitation in this area derives from biogenic methane primarily (i.e. a shallow source).

5.4. Formation mode of fluid-escape structures and links with sediment deformation

5.4.1. Lower slope

One major result of this study is the close relationship between slope parallel elongated ridges/troughs and the occurrence of fluid-escape structures (see Fig. 9; Table 3). In the lower slope, carbonate-paved areas are located clearly on top of ridges, whereas methane venting occurs above troughs (Fig. 9). It is very likely that gravity processes and deformation in the lower slope have created preferential pathways for fluid migration and gas escape. The large depressions or troughs, characterized by intense bioactivity and active methane venting, corresponds most probably to the present-day seafloor expression of those preferential pathways (e.g. faults) related to sediment deformation (Fig. 9). Pockmarks observed in close vicinity to the troughs could form from excess volumes of fluids periodically migrating upslope from the troughs, possibly aided by the creation of migration pathways along fractures (Fig. 9).

At present, it is likely that carbonate precipitation occurs within sediments in those depressions associated to active methane venting. Instead, we propose that carbonate pavements emplaced on top of ridges were outcropped on the seafloor in response to sediment instability, *after* initial formation of carbonate crusts. The exposure of those carbonate pavements could be due either to compressional deformation as pressure ridges or, alternatively, be related to faulting associated with the rotated blocks. This exhumation process would be in agreement with the presence of intensively fractured carbonate crusts on top of those ridges. Carbonate ridges would hence correspond to 'paleo-troughs' (i.e. ancient sites of active fluid venting). Our geochemical results suggest that fluid seepage at those ridges has decreased most probably since the early Holocene (see section 5.2). Most likely, this indicates that slope instability may induce a change in fluid flow conditions at any given location; from focused flow to diffuse flow for the case of those carbonate ridges. The persistence of seep habitats on top of ridges at present would hence be related to pervasive microseepage only.

Other carbonate ridges were discovered recently on the continental slope off Norway (Hovland et al., 2005), though in a different geological setting (e.g. proximity to gas hydrate reservoirs). Hovland et al. (2005) proposed that such ridges were formed during catastrophic fluid-flow events, in response to abrupt breaking of carbonate seals above preferential fluid pathways. In the Central Nile province, however, observation that carbonate ridges occur only on one side of those large sediment depressions (see bathymetric profile in Figs. 3B and C) argues against such a formation by catastrophic fluid flow event. Therefore, our preferred explanations remain that: 1) fluid migration is controlled by slope instability in the lower slope, and 2) sediment gliding is responsible for formation of carbonate ridges.

During the last few hundred thousand years, sediment mass-wasting has been active in the Nile deep sea fan, leading to deposition of a series of debris-flows and turbidites (Ducassou et al., 2007). It is likely that sediment accumulation on the middle and lower slopes has led, to some extent, to compaction/dewatering in sub-surface sediments, generating ultimately excess pore water pressure and fluid migration. Investigation of core NLK11 shows that sediments deposited above those debris-flow deposits (i.e. the top ~ 12 m of core NLK11) exhibit vertical pipes filled with fluidised sediments, which correspond to fluid migration structures (Fig. 5). In contrast, sediments associated with debris-flow deposits are highly compacted. One hypothesis would be that the upper surface of debris-flow deposits act as a décollement layer, along which fluids would migrate preferentially. The presence of such a décollement layer at a few meters below the seafloor would favour both sediment instabilities (i.e. creeping) and fluid seepage in the lower slope (Fig. 9).

5.4.2. Middle slope

Significant differences in e.g. surface, morphology, fracturation have been observed between carbonate-paved areas from the lower and middle slopes (see section 4.2), indicating that they were formed most probably through distinct processes. U/Th isotope ages calculated on authigenic carbonates recovered from the middle slope (Bayon et al., 2007) showed that fluid emission in this area (at least in that carbonate-paved area explored during dive NL7) has remained active for the last 5,000 years at least. This suggests that the middle slope has remained stable (i.e. no major slope instability) during that period. In contrast with the lower slope, the absence of any significant preferential conduits and/or faulting within surface sediments in this area may provide possibilities for broad diffusive, perhaps not focused, but permanent fluid venting through time.

5. Conclusions

Fluid venting is active on the Central Nile margin, as demonstrated by the observation of fluid-related structures (pockmarks, carbonate pavements), abundant associated chemosynthetic communities and the detection of bottom-water methane anomalies. Detailed investigations of cold seeps from two distinct areas in the Central Nile province indicate a link between fluid seepage and sediment instability.

The lower slope from 1650 m to 2200 m water depth is a zone of regional sediment creeping, where active gravitational processes create a series of elongated slope-parallel ridges and depressions. Fossil carbonate ridges up to 5m high occur on top of those slope-parallel ridges, whereas the deep depressions correspond to areas of active fluid flow. The middle slope from 700 m to 1650 m water depth corresponds to an area recently covered by debris flow deposits, which overlap surface sediments in the lower slope. In contrast with the lower slope, it shows no signs of sediment creeping, but exhibits large patchy areas (~1 km^2) of carbonate pavements associated to broad and more diffuse fluid flow.

We propose that sediment instability in the lower slope area creates preferential pathways for focused fluid flow and leads to the exposure of carbonate ridges. Evidence that debris-flow deposits buried under the destabilized sedimentary cover in this area are highly compacted may suggest that the top of this debris-flow unit acts as a décollement layer, along which fluids would migrate preferentially and, in turn, favor sediment gliding. Overall, our results have general implications for understanding the processes controlling methane fluxes at continental margins, and how slope instability may contribute to methane release into the water column.

Acknowledgements

We thank the Captains, the officers and crews of R/V *Atalante* and R/V *Pelagia*, the pilots and technicians of *Nautile*, and members of the Nautinil and Mimes scientific parties for their assistance at sea. We are grateful to P. Briand (Ifremer) for his help in identifying biological specimens. A. Mason (U. Oxford) is thanked for assistance during U/Th analyses. Two anonymous reviewers are thanked for their comments and suggestions. The Nautinil and Mimes expeditions were funded by IFREMER and the Netherlands Organization for Scientific research (NWO), respectively, as part of the MEDIFLUX Project (EUROMARGINS–ESF programme).

References

Abdel Aal, A., El Barkooky, A., Gerrits, M., Meyer, H., Schwander, M., Zaki, H.A., 2000. Tectonic evolution of the Eastern Mediterranean basin and its significance for hydrocarbon prospectivity in the ultradeepwater of the Nile delta. The Leading Edge, 1086–1102.

Allen, J.R.L., 1985. Principles of physical sedimentology. Allen and Unwin, London, 272 pp.

Bayon, G., Henderson, G.M., Bohn, M., Gontharet, S., Pierre, C., 2007. U-Th stratigraphy of a cold seep carbonate crust. Geochim. Cosmochim. Acta 71, 15, Supplement 1, A68-A68.

Bellaiche, G., Loncke, L., Gaullier, V., Mascle, J., Courp, T., Moreau, A., Radan, S., Sardou, O., 2001. Le cône sous-marin du Nil et son réseau de chenaux profonds: Nouveaux résultats (campagne Fanil). C. Rd. Ac. Sci., Paris 333, 399–404.

Borowski, W. S., Paull, C. K., Ussler III, W., 1999. Global and local variations of interstitial sulphate gradients in deep-water, continental margin sediments: Sensitivity to underlying methane and gas hydrates. Mar. Geol. 159, 131-154.

Bourdon, B., Henderson, G. M., Lundstrom, C. C., Turner, S. P., 2003. Uranium-series geochemistry. Rev. Min. Geochem. 52, 656 pp.

de Lange, G.J., Ten Haven, H.L., 1983. Recent sapropel formation in the eastern Mediterranean. Nature 305, 797-798.

Dimitrov, L., Woodside, J., 2003. Deep sea pockmarks environments in the eastern Mediterranean. Mar. Geol. 195, 263–276.

Ducassou, E., Capotondi, L., Murat, A., Bernasconi, S. M., Mulder, T., Gonthier, E., Migeon, S., Duprat, J., Giraudeau, J., Mascle, J., 2007. Multiproxy Late Quaternary stratigraphy of the Nile deep-sea turbidite system — Towards a chronology of deep-sea terrigeneous system. Sedim. Geol. 200, 1-13.

Duperron, S., Fiala-Médioni, A., Caprais, J.-C., Olu, K., Sibuet, M., 2007. Evidence for chemoautotrophic symbiosis in a Mediterranean cold seep clam (Bivalvia: Lucinidae): comparative sequence analysis of bacterial 16S rRNA, APS reductase and RubisCO genes. FEMS Microbiol. Ecol. 59, 64-70.

Duperron, S., Halary, S., Lorion, J., Sibuet, M., Gaill, F., 2008. Unexpected co occurrence of 6 bacterial symbionts in the gill of the cold seep mussel Idas sp. (Bivalvia: Mytilidae). Environ. Microbiol. 10(2), 433-445.

Dupré, S., Woodside, J., Foucher, J.-P., de Lange, G., Mascle, J., Boetius, A., Mastalerz, V., Stadnitskaia, A., Ondreas, H., Huguen, C., Caprais, J.-C., Gontharet, S., Loncke, L., Deville, E., Niemann, H., Fiala-Medioni, A., Dählmann, A., Prinzhofer, A., Sibuet, M., Pierre, C., Sinninghe Damsté, J., 2007. Seafloor geological studies above active gas chimneys off Egypt (Central Nile Deep Sea Fan). Deep-Sea Res. I 54, 1146-1172.

Gaullier, V., Mart, Y., Bellaiche, G., Mascle, J., Vendeville, B., Zitter, T., the Prismed Scientific Party, 2000. Salt tectonics in and around the Nile deep sea fan : insights from the Prismed II cruise. In: Vendeville, B., Mart, Y., Vigeresse, J.L. (eds.) Salt, Shale and Igneous diapirs in and around Europe. Geological Society, London, Spec. Pub. 174, 110-129.

Gay, A., Lopez, M., Cochonat, P., Sermondadaz, G., 2004. Polygonal faults–troughs system related to early stages of compaction—Upper Miocene to present sediments of the Lower Congo Basin. Basin Res. 16, 101–116.

Gay, A., Lopez, M., Cochonat, P., Séranne, M., Levaché, D., Sermondadaz, G., 2006. Isolated seafloor pockmarks linked to BSRs, fluid chimneys, polygonal faults and stacked Oligocene–Miocene turbiditic palaeochannels in the Lower Congo Basin. Mar. Geol. 226, 25-40.

Gontharet, S., Pierre, C., Blanc-Valleron, M.M., Rouchy, J.M., Fouquet, Y., Bayon, G., Foucher, J.P., Woodside, J., Mascle, J., the Nautinil scientific party, 2007. Nature and origin of the diagenetic carbonate crusts and concretions from mud volcanoes and pockmarks of the Nile deep-sea fan (eastern Mediterranean sea). Deep-Sea Res. II 54, 1291-1316.

Haese, R. R., Meile, C., van Cappellen, P., de Lange, G. J., 2003. Carbon geochemistry of cold seeps: Methane fluxes and transformation in sediments from Kazan mud volcano, eastern Mediterranean Sea. Earth Planet. Sci. Let. 212, 361-375.

Hovland, M., Judd, A.G., 1988. Seabed Pockmarks and Seepages: Impact on Geology, Biology and Marine Environment vol. 293, Graham and Trotman, London, 565 pp.

Hovland, M., Gardner, J.V., Judd, A.G., 2002. The significance of pockmarks to understanding fluid flow processes and geohazards. Geofluids 2, 127–136.

Hovland, M., Svensen, H., Forsberg, C.F., Johansen, H., Fichler, C., Fosså, J.H., Jonsson, R., Rueslåtten, H., 2005. Complex pockmarks with carbonate-ridges off mid-Norway: Products of sediment degassing. Mar. Geol. 218, 191-206.

Huguen, C., Foucher, J.-P., Mascle, J., Ondreas, H., Thouement, M., Gontharet, S., Stadnitskaia, A., Pierre, C., Bayon, G., Loncke, L., Boetius, A., Bouloubassi, I., de Lange, G., Caprais, J.-C., Fouquet, Y., Woodside, J., and the NAUTINIL Scientific Party, 2008. Menes Caldera, a highly active site of brine seepage in the Eastern Mediterranean Sea: "in situ" observations from the Nautinil expedition (2003). Marine Geology (EUROMARGINS Special Issue, **This volume**).

Judd, A.G., Hovland, M., 2007. Seabed Fluid Flow, the impact on geology, biology and the marine environment. Cambridge University Press, 475 pp.

Kennett, J. P., Cannariato, K. G., Hendy, I. L., Behl, R. J., 2002. Methane hydrates in quaternary climate change: the clathrate gun hypothesis. Am. Geophys. Union, 216 pp.

Lastras, G., Canals, M., Urgeles, R., Hughes-Clarke, J.-E., Acosta, J., 2004. Shallow slides and pockmark swarms in the Eivissia Channel, western Mediterranean Sea. Sedimentology 51, 1–14.

Lee, S.H., Chough, S.K., 2001. High-resolution (2±7 kHz) acoustic and geometric characters of submarine creep deposits in the South Korea Plateau, East Sea. Sedimentology 48, 629-644.

Loncke, L., Gaullier, V., Bellaiche, G. and Mascle, J., 2002. Recent depositional patterns of the Nile Deep-Sea Fan from echo-character mapping. AAPG Bull. 86, 1165–1186.

Loncke, L., Mascle, J., Fanil Science Party, 2004. Mud volcanoes, gas chimneys pockmarks and ridges in the Nile deep-sea fan (Eastern Mediterranean): geophysical evidences. Mar. Petrol. Geol. 21, 669–689.

Loncke, L., Gaullier, V., Mascle, J., Vendeville, B., Camera, L., 2006. The Nile deep-sea fan : An example of interacting sedimentation, salt tectonics, and inherited subsalt paleotopographic features. Mar. Petrol. Geol. 23, 297-315.

Mascle, J., Benkhelil, J., Bellaiche, G., Zitter, T., Woodside, J., Loncke, L. and Prismed II scientific party, 2000. Marine geological evidence for a Levantine–Sinai plate, a missing piece of the Mediterranean puzzle. Geology 28, 779–782.

Maslin, M.A., Owen, M., Day, S., Long, D., 2004. Linking continental slope failure to climate change: Testing the Clathrate Gun Hypothesis. Geology 32, 53-56.

Mienert, J., 2004. COSTA—continental slope stability: major aims and topics. Mar. Geol. 213, 1-7.

Mienert, J., Vanneste, M., Bünz, S., Andreassen, K., Haflidason, H., Sejrup, H.P., 2005. Ocean warming and gas hydrate stability on the mid-Norwegian margin at the Storegga Slide. Mar. Petrol. Geol. 22, 233-244

Mulder, T., Cochonat, P., 1996. Classification of offshore mass movements. J. Sedim. Res. 66, 43-57.

Niewöhner, C., Hensen, C., Kasten, S., Zabel, M., Schulz, H. D., 1998. Deep sulphate reduction completely mediated by anaerobic methane oxidation in sediments of the upwelling area off Namibia. Geochim. Cosmochim. Acta 62, 455-464.

Nisbet, E.G., 2002. Have sudden large releases of methane from geological reservoirs occurred since the Last Glacial Maximum, and could such releases occur again? Phil. Trans. R. Soc. Lond. A 360, 581-607.

Olausson, E., 1961. Studies of deep sea cores. Reports of Swedish Deep-Sea expeditions 1947-1948, 8, 336-391.

Olu-Le Roy, K., Sibuet, M., Fiala-Médioni, A., Gofas, S., Salas, C., Mariotti, A., Foucher, J.P., Woodside, J., 2004. Cold seep communities in the deep eastern Mediterranean Sea: composition, symbiosis and spatial distribution on mud volcanoes. Deep-Sea Res. I 51, 1915-1936.

Paull, C.K., Ussler III, W., Dillon, W.P., 2000. Potential role of gas hydrate decomposition in generating submarine slope failures. In: Max, M.D. (Ed.), Natural Gas Hydrate in Oceanic and Permafrost Environments, Kleuwer Acad. Publishers, Dordrecht, 149–156.

Paull, C., Ussler III, W., Maher, N., Greene, H.G., Rehder, G., Lorenson, T., Lee, H., 2002. Pockmarks off Big Sur, California. Mar. Geol. 181, 323–335.

Pickering, K.T., Hiscott, R.N., and Hein, F.J., 1989. Deep marine environments. Harper-Collins, London, 416 pp.

Rossignol-Strick, M., Nesteroff, W.D., Olive, P., Vergnaud-Grazzini C., 1982. After the deluge: Mediterranean stagnation and sapropel formation. Nature 295, 105-110.

Salas, C., Woodside, J., 2002. *Lucinoma kazani* n. sp. (Mollusca: Bivalvia): evidence of a living benthic community associated with a cold seep in the Eastern Mediterranean Sea. Deep-Sea Res. I 49, 991-1005.

Salem, R., 1976. Evolution of Eocene–Miocene sedimentation patterns in parts of Northern Egypt. AAPG Bull. 60, 34–64.

Samuel, A., Kneller, B., Raslan, S., Sharp, A. and Parsons, C., 2003. Prolific deep-marine slope channels of the Nile delta, Egypt. AAPG Bull. 87, 541–560.

Sardou, O., Mascle, J., 2003. Cartography by multibeam echo-sounder of the Nile deep-sea Fan and surrounding areas (2 sheets). Special publication CIESM, Monaco.

Sowers, T., 2006. Late Quaternary atmospheric CH4 isotope records suggests marine clathrates are stable. Nature 311, 838-840.

Stow, D.A.V., 1994. Deep-sea processes of sediment transport and deposition. In: Pye, K. (Ed.), Sediment Transport and Depositional Processes. Blackwell, London, pp. 257-293.

Sturany, R., 1896. Zoologische Ergebnisse VII. Mollusken I (Prosobranchier und Opisthobranchier; Scaphopoden; Lamellibranchier) gesammelt von S.M. Schiff "Pola" 1890-1894. Denkschriften der Kaiserlichen Akademie der Wissenschaften, Mathematische-Naturwissenschaftlischen Classe 63, 1-36, pl.1-2.

Teichert, B. M. A., Eisenhauer, A., Bohrmann, G., Haase-Schramm, A., Bock, B., Linke, P., 2003. U/Th systematics and ages of authigenic carbonates from Hydrate Ridge, Cascadia Margin: recorders of fluid flow variations. Geochim. Cosmochim. Acta 67, 3845-3857.

Trincardi, F., Cattaneo, A., Correggiari, A., Ridente, D., 2004. Evidence of soft sediment deformation, fluid escape, sediment failure and regional weak layers within the late Quaternary mud deposits of the Adriatic Sea. Mar. Geol. 213, 91-119.

Ussler III, W., Paull, C.K., Boucher, J., Friederich, G.E., Thomas, D.J., 2003. Submarine pockmarks: a case study from Belfast Bay, Maine. Mar. Geol. 202, 175–192.

van Weering, T.C.E., Nielsen, T., Kenyon, N.H., Akentieva, A.K., Kuijpers, A. 1998. Large Submarine slides at the NE Faroe continental margin. In: Stoker, M., Evans, D., and Cramp, R. (Eds.), Geological Processes on Continental Margins: Sedimentation, Mass-Wasting and Stability. Geological Society London Special Publications 129, pp. 5-17.

Vogt, P.R., Gardner, J., Crane, K., Sundvor, E., Bowles, F., Cherkashev, G., 1999. Ground-truthing 11- to 12-kHz side-scan sonar imagery in the Norwegian–Greenland Sea. Part I: pockmarks on the Vestnesa Ridge and Storegga slide margin. Geo Mar. Lett. 19, 97–110.

Webb, M., 1969. *Lamellibrachia barhami* gen. nov. sp. nov., (Pogonophora) from the northeast Pacific. Bull. Mar. Sci. 19, 18–47.

Figure Captions

Figure 1: Bathymetric map of the Nile deep-sea fan (Sardou and Mascle, 2003) and distribution of fluid-escape structures (Loncke et al., 2004) showing the two sites investigated with the *Nautile* submersible, at 2100 m depth (lower slope) and 1650 m depth (middle slope). Note the presence of elongated ridges sub-parallel to the slope (direction ~ N70) in the lower slope of the Central Province.

Figure 2: (A) 3.5-kHz sub-bottom profile perpendicular to the slope in the Central Nile Province (see Fig. 1 for NL2-6 trackline position). (B,C) Shaded bathymetric maps of the two sites investigated in the Central Nile Province with position of the *Nautile* transects (see location of sites in Fig. 1). (B) Middle slope, dive NL7, 1650 m water depth; (C) Lower slope, dives NL6 and NL14, 2100 m water depth. Note the marked morphological contrast between the middle slope and the lower slope. The lower slope is characterised by a rough and morphological seafloor morphology, which exhibits repeated elongated ridges and depressions parallel to the slope.

Figure 3: Seafloor observations of fluid-escape structures in the lower slope domain. (A) Multibeam seafloor acoustic imagery showing the distribution of highly reflective patches (dark spots) with indication of the *Nautile* transects (see location of sites in Fig. 1). (B,C) Maps for sediment and carbonate facies, microbathymetric profiles and bottom-water methane anomalies recorded along the dive transects. Fault positions and sampling sites for sediment cores and carbonate crusts are also shown.

Figure 4: Side-scan sonar image of the seafloor in the middle slope showing the presence of large carbonate paved-areas with indication of the *Nautile* transect (see location in Fig. 1). Sampling sites for sediment cores and carbonate crusts collected during the dive are also reported.

Figure 5: Lithological description of sediment cores recovered during the submersible dives. Push cores NL6-PC1, NL14-PC1 and NL14-PC3 were collected in the lower slope, in fluid-venting areas (pockmark, carbonate ridges). Box core NL7-BC1 was recovered in the middle slope, away from any fluid-escape structure. The location of these cores is shown in Figs. 1, 3B,C, and 4.

Figure 6: Seafloor bottom photographs of fluid-escape structures. (A) Carbonate pavements partly covered by thin sediments (carbonate ridge; lower slope). (B) Fractured carbonates on a carbonate ridge (lower slope). (C) Fracture on a carbonate ridge (lower slope). (D) Non fractured massive carbonate pavement (middle slope). (E) Small pockmark (~ 3 m across) in the lower slope. Note the presence of authigenic carbonates, grey anoxic sediments and vestimentiferan tubeworms. (F) Large pockmark (~ 25 m across) exhibiting two carbonate chimneys and a dense network of infilled burrows (middle slope). The central part of the pockmark corresponds to accumulated debris of dead shells, authigenic carbonates and burrows. (G) Shell-rich sediments and bioturbation mounds in one of those troughs (large seafloor depression) related to gravity tectonics

(lower slope). (H) Fault in hemipelagic sediments away from fluid-escape structures (lower slope). White scale bars correspond to ~ 1 m.

Figure 7: Vestimentiferan tubeworms associated with carbonate crusts. (A) First morphotype observed, assigned preliminarily to the genus *Lamellibrachia* (dive NL7; middle slope). (B) Second morphotype observed, but not collected (dive NL6; lower slope). Note that the morphology of the chitinous tube differs from that of the first morphotype. White scale bars correspond to ~ 20 cm.

Figure 8: Down-core profiles of CaO (wt%), $S_{oxidized}$ (wt%), $S_{reduced}$ (wt%), Ba (ppm) for push-cores NL14-PC1 and NL14-PC3 taken at a carbonate ridge (lower slope, see location in Figs. 3B and C). Dissolved pore water SO_4^{2-} (mM) contents are also plotted for core NL14-PC1. Enrichments of oxidized/reduced sulphur and barium in solid sediment phases indicate that reduction of dissolved sulphates has been active at these locations in the recent past. In contrast, the flat dissolved SO_4^{2-} profile, with seawater-like values, shows that sulphate reduction does not take place in sub-surface sediments at present.

Figure 9: Conceptual model linking fluid seepage and sediment deformation in the lower slope. Active gravitational processes (creep and/or gliding) create a series of elongated slope-parallel sediment ridges and depressions in the lower slope. Sediment instability leads to exhumation of fractured carbonate pavements on top of ridges, which correspond to ‘fossil’ vent sites. The exhumation of those carbonate ridges can be due either to

compressional deformation (i.e. creep) or be related to faulting associated with rotated blocks (i.e. gliding). The depressions correspond instead to preferential pathways for focused fluid flow. The top of debris-flow deposits (highly compacted) buried under the destabilized sediment cover could act as a décollement layer along which fluids would migrate preferentially, favouring in turn sediment gliding.

Table 1. Positions and water depths of the cores and carbonate crusts investigated

Core / Carbonate	Description	Length (m)	Water depth (m)	Latitude N	Longitude E
Sediment cores					
NL6-PC1	Push core	0.36	2115	32°38.14'	29°56.12'
NL14-PC1	Push core	0.35	2116	32°38.33'	29°55.80'
NL14-PC3	Push core	0.25	2130	32°38.44'	29°54.98'
NLK11	Kullenberg	14	2207	32°40.99'	29°54.00'
NL7-BC1	Blade core	0.15	1623	32°30.50'	30°23.09'
Carbonate crusts					
NL6-CC1	lithified crust		2132	32°38.38'	29°54.87'
NL14-CC5	lithified crust		2130	32°38.44'	29°54.98'
NL7-CC2	porous crust		1686	32°31.61'	30°21.16'

Table 2. U-Th data for authigenic carbonates

Sample	Depth (cm)	^{238}U (ppm)	^{230}Th (ppt)	$(^{230}Th/^{232}Th)$	$\delta^{234}U_{(0)}$	Isochron age (ka)
NL14-CC5	0.5	2.997 ± 0.004	28.67 ± 0.14	2.44 ± 0.01	128.7 ± 1.7	-
'	2	5.158 ± 0.006	17.15 ± 0.04	3.62 ± 0.01	144.2 ± 1.7	7.9 ± 1.4
NL6-CC1	2	3.702 ± 0.004	35.29 ± 0.15	2.52 ± 0.01	129.3 ± 1.7	-

Table 3. Geological setting and fluid-vent structures in the lower and middle slope

	Lower slope	Middle slope
Geological setting	▪ Debris-flow deposits overlain by a 'thick' creeping hemipelagic cover (~15 m)	▪ Debris-flow deposits overlain by 'thin' hemipelagic cover (~ 0.5 m)
Seafloor surface	▪ Rough (ridges and troughs)	▪ Flat
Gravitational processes	▪ Active creeping processes leading to formation of ridges and throughs ▪ Extensional regime mainly (rotated blocks) ▪ Probably local compressive ridges distally and above irregularities of decollement plane	▪ Not active at present ▪ Uniformaly disorganised debris-flow deposits
Fluid-vent structures	▪ Carbonate ridges (~500 m long) associated with compressional ridges ▪ Throughs (methane emission) ▪ Small pockmarks	▪ Large carbonate-paved areas (> 1 km^2) with irregular shapes ▪ Pockmarks
Degree of seepage activity	▪ Reduced activity at carbonate ridges ▪ Active methane venting above furrows	▪ Continuous activity for at least the last ~5 kyr

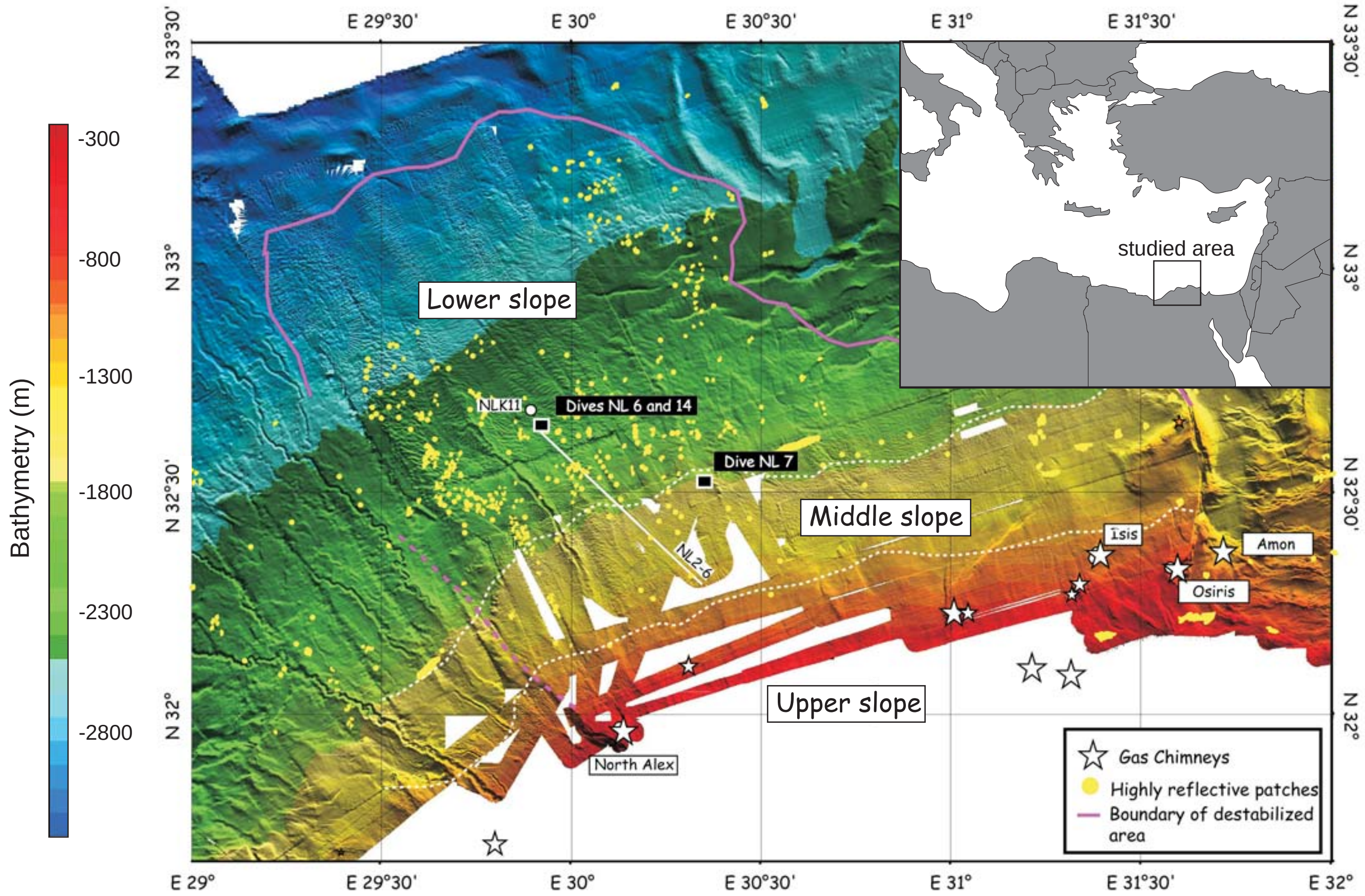

Bathymetry (m)
-300
-800
-1300
-1800
-2300
-2800
E 29°30'
E 30°
E 30°30'
E 31°
E 31°30'
E 29°
E 32°
N 33°30'
N 33°
N 32°30'
N 32°
Lower slope
Middle slope
Upper slope
NLK11
Dives NL 6 and 14
Dive NL 7
NL2-6
North Alex
Isis
Amon
Osiris
studied area
Gas Chimneys
Highly reflective patches
Boundary of destabilized area

Fig1

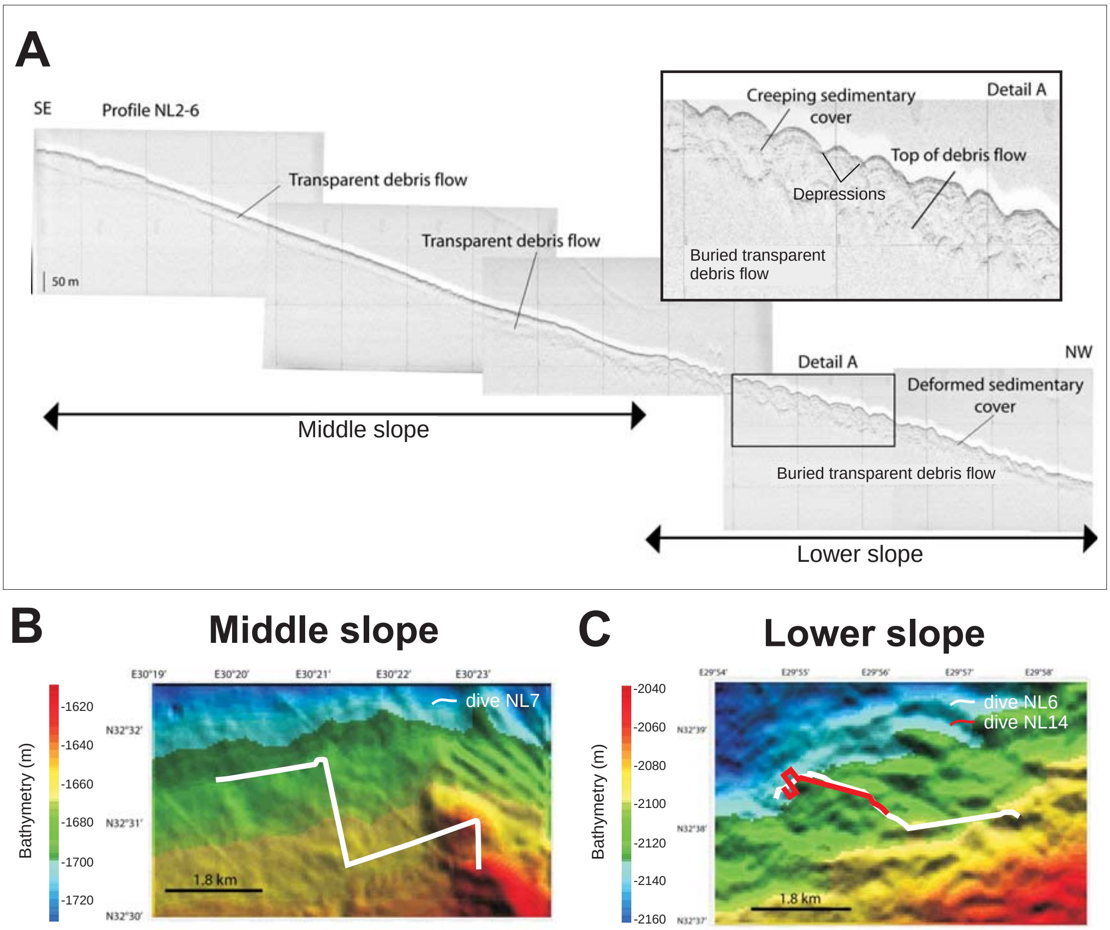
A
SE
Profile NL2-6
Transparent debris flow
Transparent debris flow
50 m
Creeping sedimentary cover
Detail A
Top of debris flow
Depressions
Buried transparent debris flow
Detail A
NW
Deformed sedimentary cover
Buried transparent debris flow
Middle slope
Lower slope
B
Middle slope
Bathymetry (m)
-1620
-1640
-1660
-1680
-1700
-1720
E30°19'
E30°20'
E30°21'
E30°22'
E30°23'
N32°32'
N32°31'
N32°30'
dive NL7
1.8 km
C
Lower slope
Bathymetry (m)
-2040
-2060
-2080
-2100
-2120
-2140
-2160
dive NL6
dive NL14
1.8 km

Fig2

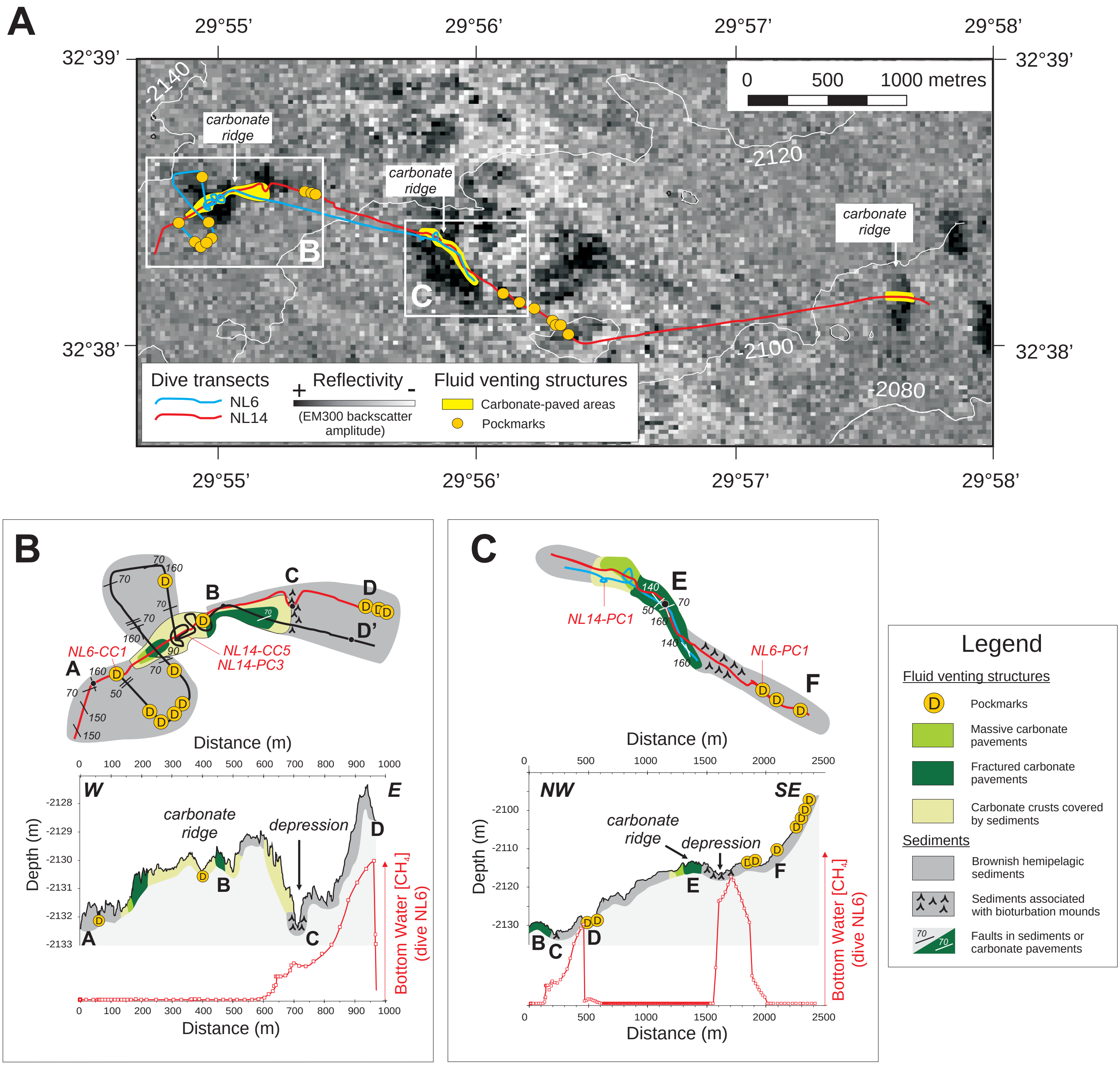
A
29°55'
29°56'
29°57'
29°58'
32°39'
32°38'
0 500 1000 metres
-2140
-2120
-2100
-2080
carbonate ridge
B
C
Dive transects
NL6
NL14
Reflectivity
+ -
(EM300 backscatter amplitude)
Fluid venting structures
Carbonate-paved areas
Pockmarks
B
NL6-CC1
NL14-CC5
NL14-PC3
Distance (m)
Depth (m)
W
E
carbonate ridge
depression
Bottom Water [CH4] (dive NL6)
C
NL14-PC1
NL6-PC1
NW
SE
Legend
Fluid venting structures
Pockmarks
Massive carbonate pavements
Fractured carbonate pavements
Carbonate crusts covered by sediments
Sediments
Brownish hemipelagic sediments
Sediments associated with bioturbation mounds
Faults in sediments or carbonate pavements

Fig3

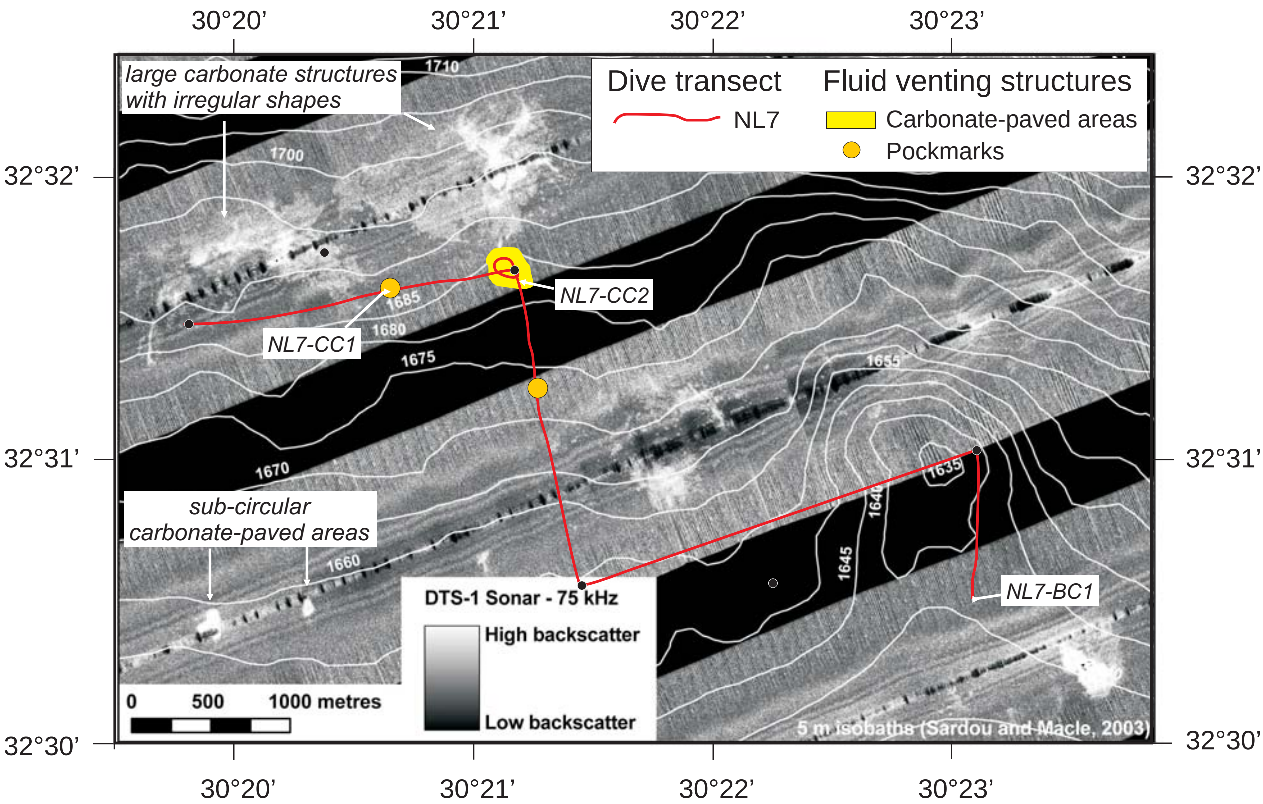

30°20'
30°21'
30°22'
30°23'
32°32'
32°31'
32°30'
large carbonate structures with irregular shapes
sub-circular carbonate-paved areas
Dive transect
NL7
Fluid venting structures
Carbonate-paved areas
Pockmarks
NL7-CC1
NL7-CC2
NL7-BC1
1710
1700
1685
1680
1675
1670
1660
1655
1645
1640
1635
DTS-1 Sonar - 75 kHz
High backscatter
Low backscatter
0
500
1000 metres
5 m isobaths (Sardou and Mascle, 2003)

Fig4

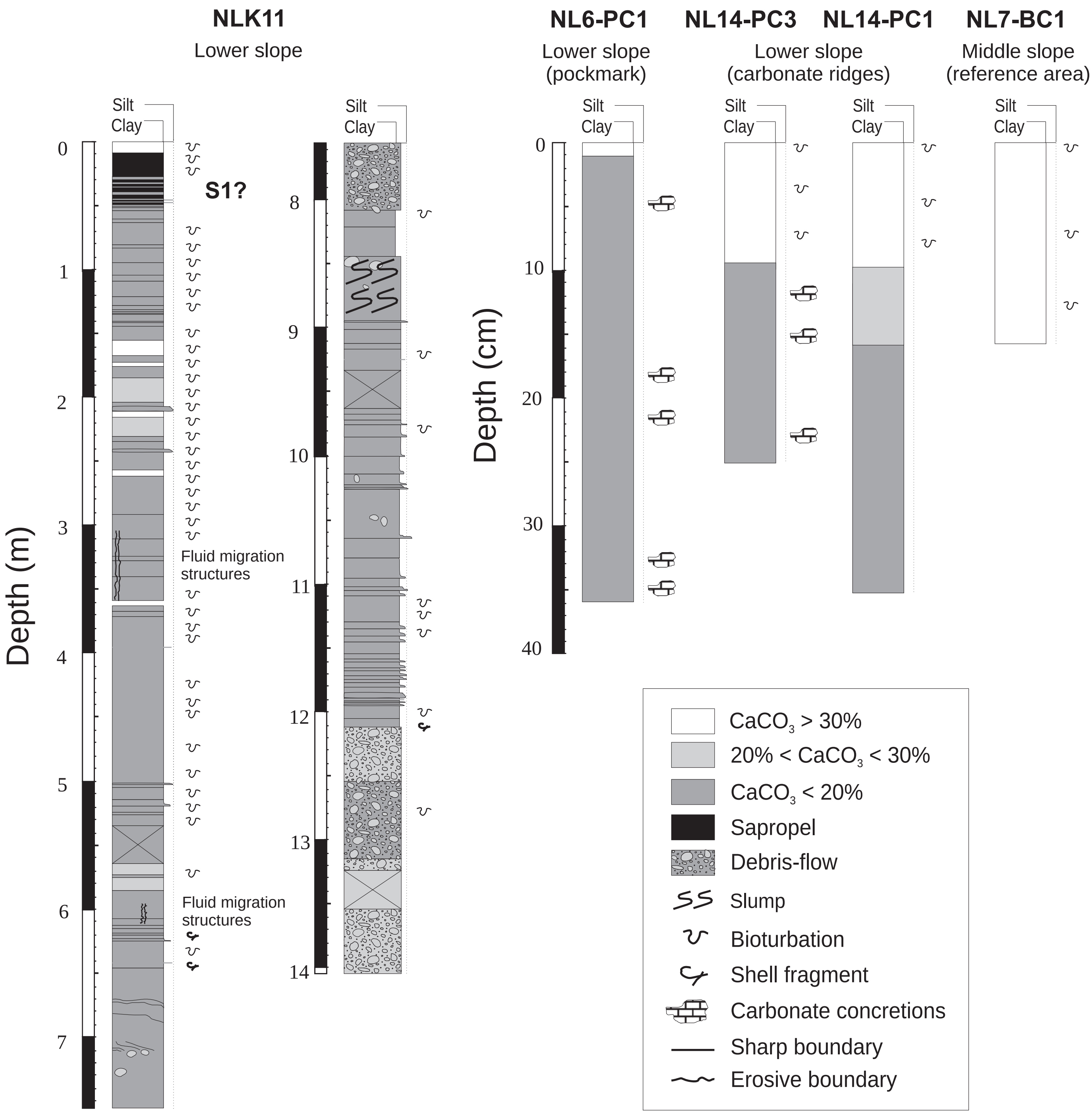

NLK11
Lower slope
NL6-PC1
Lower slope (pockmark)
NL14-PC3
NL14-PC1
Lower slope (carbonate ridges)
NL7-BC1
Middle slope (reference area)
Silt
Clay
Depth (m)
Depth (cm)
S1?
Fluid migration structures
CaCO3 > 30%
20% < CaCO3 < 30%
CaCO3 < 20%
Sapropel
Debris-flow
Slump
Bioturbation
Shell fragment
Carbonate concretions
Sharp boundary
Erosive boundary

Fig5

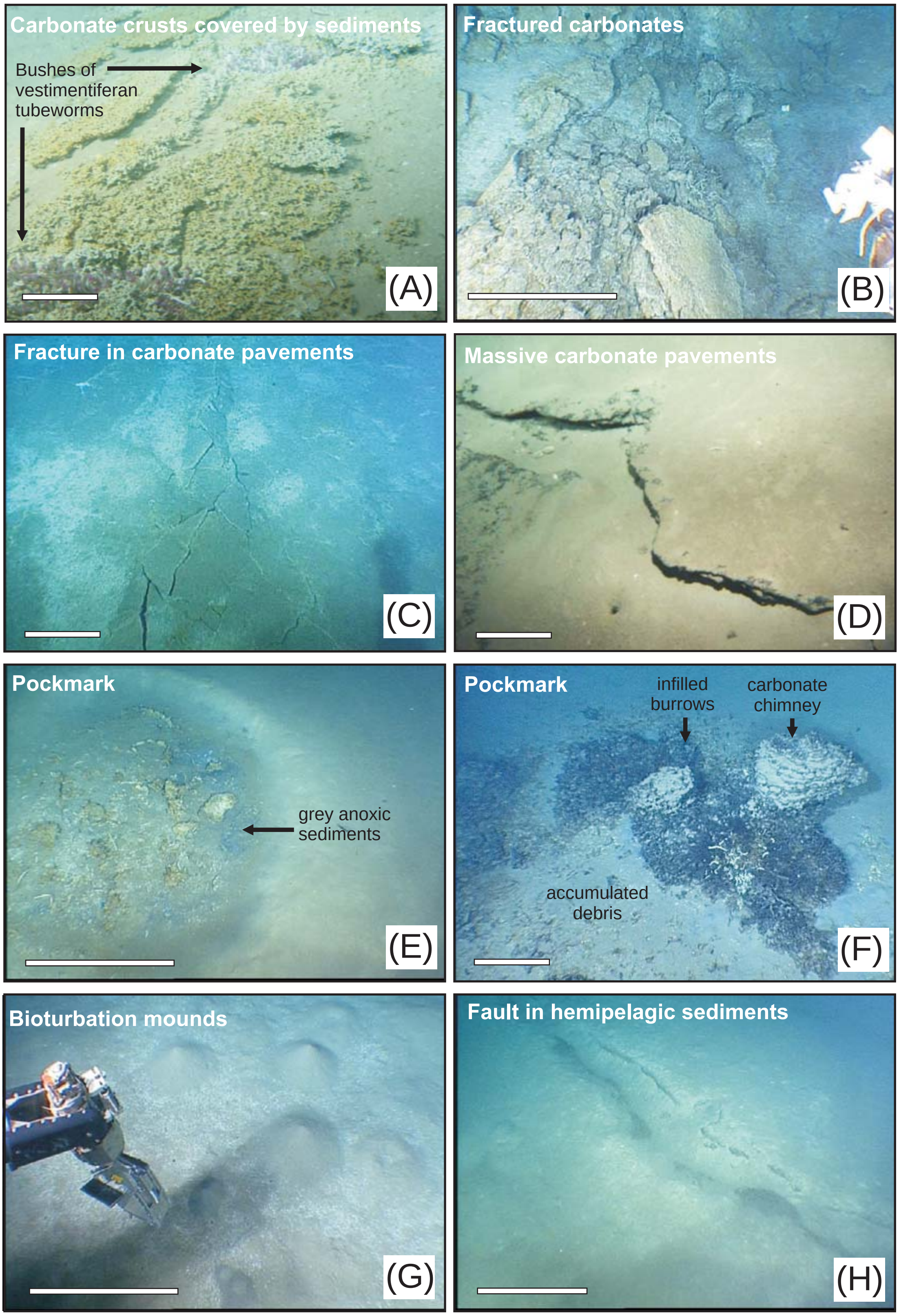
Carbonate crusts covered by sediments
Bushes of vestimentiferan tubeworms
(A)
Fractured carbonates
(B)
Fracture in carbonate pavements
(C)
Massive carbonate pavements
(D)
Pockmark
grey anoxic sediments
(E)
Pockmark
infilled burrows
carbonate chimney
accumulated debris
(F)
Bioturbation mounds
(G)
Fault in hemipelagic sediments
(H)

Fig6

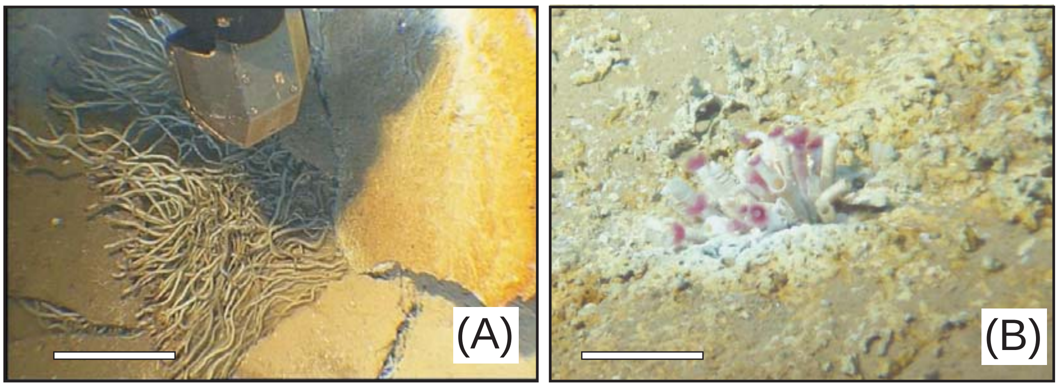

Fig7

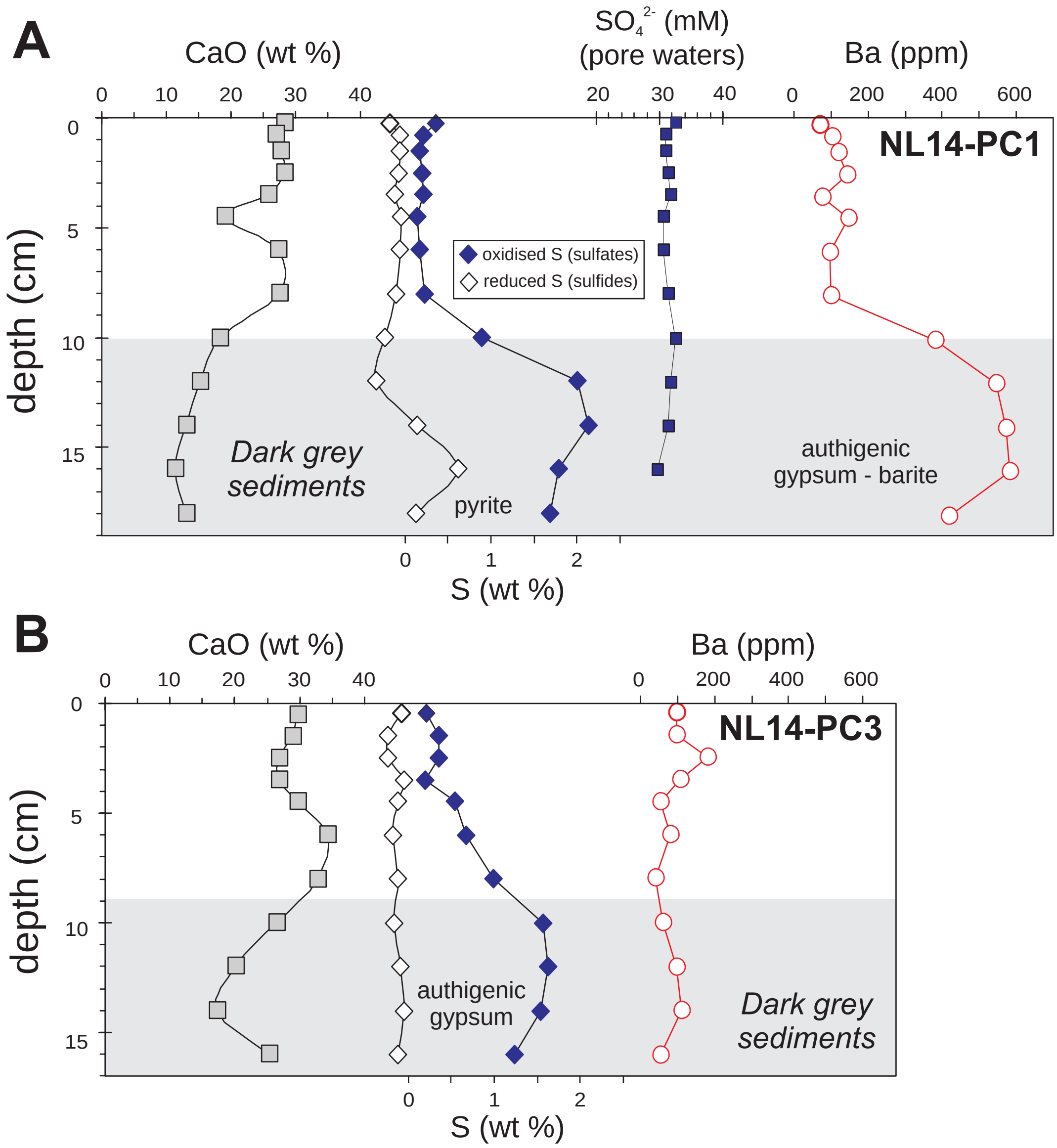
A
CaO (wt %)
SO$_4^{2-}$ (mM)
(pore waters)
Ba (ppm)
NL14-PC1
depth (cm)
oxidised S (sulfates)
reduced S (sulfides)
Dark grey
sediments
pyrite
authigenic
gypsum - barite
S (wt %)
B
CaO (wt %)
Ba (ppm)
NL14-PC3
depth (cm)
authigenic
gypsum
Dark grey
sediments
S (wt %)

Fig8

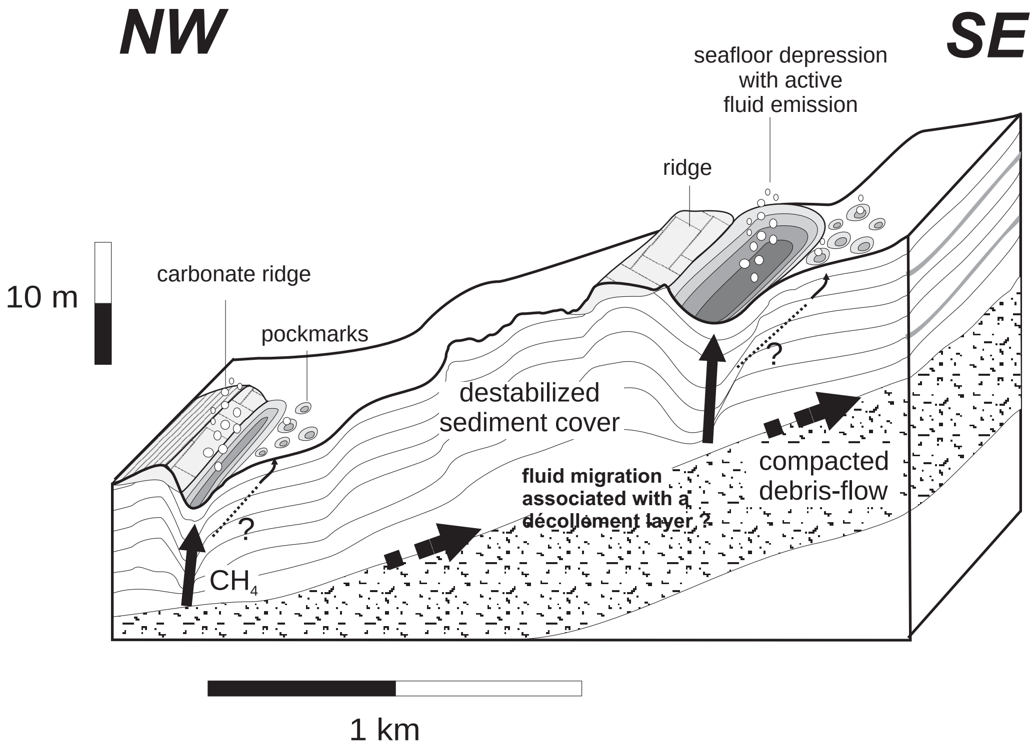
NW
SE
seafloor depression
with active
fluid emission
ridge
carbonate ridge
10 m
pockmarks
destabilized
sediment cover
?
?
fluid migration
associated with a
décollement layer ?
compacted
debris-flow
CH4
1 km

Fig9